Draft version October 23, 2013
Preprint typeset using LaTeX style emulateapj v. 5/2/11

ON THE MINIMUM CORE MASS FOR GIANT PLANET FORMATION AT WIDE SEPARATIONS

Ana-Maria A. Piso
Harvard-Smithsonian Center for Astrophysics

Andrew N. Youdin
JILA, University of Colorado at Boulder
Draft version October 23, 2013

ABSTRACT

The core accretion hypothesis proposes that giant planets form by the accretion of gas onto a solid protoplanetary core. The minimum (or critical) core mass to form a gas giant is typically quoted as $10M_\oplus$. This value, however, depends on several factors, such as the location in the disk, atmospheric opacity, and the accretion rate of solids. Motivated by ongoing direct imaging searches for giant planets, this study focuses on core mass requirements in the outer disk. Our model investigates the growth of atmospheres around solid cores of fixed mass. Without planetesimal accretion to heat the atmosphere, our limiting case gives the fastest possible atmospheric growth by Kelvin-Helmholtz contraction. We develop a two-layer, spherical atmosphere model with an inner convective region and an outer radiative zone that matches onto the protoplanetary disk. For different locations in the disk, we determine the minimum core mass for a giant planet to form within a typical disk lifetime of 3 Myr. The minimum core mass required to nucleate atmosphere collapse is $\sim 8M_\oplus$ at 5 AU and steadily decreases to $\sim 3.5M_\oplus$ at 100 AU, for a solar composition atmosphere with a standard ISM dust opacity. This trend is mainly explained by the cooler temperatures in the outer disk. Lower pressure and densities in the outer disk have a negligible effect on core mass requirements. At all distances, decreasing the dust opacity and/or increasing the mean molecular weight of the atmosphere reduces the critical core mass. The ongoing accretion of solids would delay or prevent atmospheric runaway growth. Thus our low values for minimum core masses do not contradict the existence of ice giants, but emphasize the importance of the accretion history of solids. We also develop a non-self-gravitating, analytic cooling model to help explain our numerical trends. Additionally, this comparison reveals that self-gravity significantly affects atmospheric evolution even when the atmosphere is only $\sim 20\%$ as massive as the core.

1. INTRODUCTION

Current theories postulate that giant planets form either through gravitational instability (GI) or core accretion (e.g., D'Angelo et al. 2011, Youdin & Kenyon 2013). In the core accretion model (e.g., Harris 1978, Mizuno et al. 1978, Stevenson 1982, Bodenheimer & Pollack 1986, Pollack et al. 1996), solid planetesimals collide and grow into a massive solid core which then accretes a gaseous envelope. GI theories postulate that giant planets can be formed due to the fragmentation of the protoplanetary disk into self-gravitating clumps (e.g., Boss 1997).

Forming giant planets at wide separations in the protoplanetary disk poses theoretical challenges. Even though GI works better at large distances than in the inner disk (e.g., Rafikov 2005), fine-tuning is still required in terms of disk conditions and infall history for planetary mass objects to be the outcome of GI (Kratter et al. 2010). On the other hand, the time to accrete the solid core is too long in the outer disk. Some models, however, allow for rapid accretion of solids even at large separations (e.g., Dones & Tremaine 1993, Kenyon & Bromley 2009, Lambrechts & Johansen 2012). We thus consider the timescale constraints imposed by the accretion of the gaseous atmosphere before the protoplanetary disk dissipates.

Several types of core accretion models have been studied previously. In static models, which are mostly analytic, the accretion rate of planetesimals regulates the growth of the atmosphere (e.g., Stevenson 1982, Rafikov 2006). The luminosity of the gaseous envelope is thus entirely supplied by planetesimal accretion. These studies consider that the atmosphere is in a steady state at all times, in which all the incoming energy from planetesimal accretion is radiated away by the envelope. For a fixed planetesimal accretion rate, the atmosphere mass grows non-linearly as the core mass increases. As the atmosphere mass becomes comparable to the mass of the solid core, hydrostatic balance no longer holds and the static model breaks down. Unstable collapse occurs if the core mass further increases, a process known as the "core accretion instability". The maximum core mass for which the atmosphere is still in hydrostatic equilibrium is defined as the "critical core mass". Typically, the critical core mass is found to be about $10M_\oplus$ (e.g., Stevenson 1982, Rafikov 2006).

Full time-dependent simulations of giant planet evolution take into account the Kelvin-Helmholtz (KH) contraction of the gaseous envelope. As a result, the atmosphere is no longer in a steady state, but rather it accretes gas as it cools radiatively. In this scenario there are two main sources that contribute to the luminosity evolution of the envelope — planetesimal accretion and gas contraction. These evolutionary models for core and atmosphere growth include time-dependent planetesimal

accretion rates that are determined by the distribution of solids in the disk, as well as the planet mass and capture cross-section. This is is contrast with the static models in which the planetesimal accretion rate is usually constant with time. Pollack et al. (1996) find that the planet growth can be separated into three relatively well defined phases. Phase 1 is dominated by the growth of the core due to runaway planetesimal accretion, and ends when the planet's feeding zone has been depleted of solids. At this stage, planetesimal accretion can no longer balance radiative losses, and the atmosphere cools and contracts. This is phase 2, during which the envelope mass steadily increases, while core growth is no longer significant. Once the atmosphere mass becomes comparable to the core mass, growth is continually accelerated, leading to runaway gas accretion, i.e. phase 3. Phase 2 is found to be much longer than the other two phases (see also Alibert et al. 2005), hence the evolutionary timescale of the atmosphere is set by KH contraction.

Since KH contraction dominates the envelope accretion timescale in many core accretion models, it is useful to study atmospheric growth onto a core of fixed mass (Ikoma et al. 2000, Papaloizou & Nelson 2005). This regime is the one considered in this work. We explore the atmosphere evolution around fully grown cores of different masses, and determine the minimum core mass to form a giant planet before disk dissipation for a variety of disk conditions and properties of the nebular gas. We note that our models are a special case of the time-dependent studies, with the planetesimal accretion rate set to zero. Our neglect of planetesimal accretion allows us to obtain absolute lower limits on the core mass needed to form a gas giant, as additional heat sources limit the ability of the atmosphere to cool and undergo KH contraction.

This paper is organized as follows. In section §2 we describe the assumptions of our atmosphere model, and derive the basic equations that govern the structure and evolution of the atmosphere. In section §3, we present a simplified analytic model that predicts the qualitative behavior of the numerical model. We describe our numerical results in section §4, and determine the critical core mass for planet formation during the life time of the protoplanetary disk in section §5. We discuss some of the approximations of our model in section §6 and summarize our findings in section §7.

2. ATMOSPHERE MODELS

To model the growth of planetary atmospheres around a solid core, we develop a simplified two-layer model for time-dependent atmospheric cooling, i.e. KH contraction. With a convective interior and radiative exterior, this model is motivated by similar models of hot Jupiters (Arras & Bildsten 2006; Youdin & Mitchell 2010).

Our model can accurately model the growth of the atmosphere up to the crossover mass, when the atmosphere mass equals the mass of the core. Beyond the crossover mass, our approximate treatment of the radiative zone (explained below) breaks down. Since subsequent growth is a rapid runaway process (e.g., Pollack et al. 1996), our model can investigate to good accuracy the timescale requirement of core accretion. Our simplified treatment is also inappropriate for hot, short-period planets, where dust sublimation gives deeper radiative zones that require more detailed models.

Our main assumptions are summarized as follows:

1. The atmosphere is spherically symmetric and remains in hydrostatic balance during its thermal evolution.
2. The core mass and radius are fixed in evolutionary calculations, neglecting ongoing planetesimal or dust accretion.
3. At the planet's Hill radius, the atmospheric temperature and pressure match the conditions of the disk midplane.
4. The only source of planetary luminosity is the gravitational contraction of the atmosphere.
5. Cooling of the atmosphere is dominated by the convective interior. Thus the luminosity in the radiative exterior is held spatially constant.
6. A global cooling model connects independent static solutions into a time-dependent sequence.
7. A polytropic equation of state (EOS) is assumed for simplicity.
8. Dust grains provide the opacity in the radiative zone, which remains cool enough to avoid dust sublimation.
9. Because gas accretion accelerates after the crossover mass, the time to reach the crossover mass, i.e. the crossover time, is a good approximation of the total time to form a gas giant.

The remainder of this section develops our model in more detail.

2.1. *Disk and Opacity Model*

We adopt a minimum mass solar nebula (MMSN) model for a passively irradiated disk (Chiang & Youdin 2010). With the semimajor axis a normalized to the outer disk as $a_{10} = a/(10\ \mathrm{AU})$, the gas surface density and mid-plane temperature are

$$\Sigma_\mathrm{d} = 70\, F_\Sigma a_{10}^{-3/2}\ \mathrm{g\ cm^{-2}} \tag{1a}$$

$$T_\mathrm{d} = 45\, F_T\, a_{10}^{-3/7}\ \mathrm{K}\,. \tag{1b}$$

The normalization factors F_Σ and F_T adjust the model relative to the fiducial MMSN. We fix $F_\Sigma = F_T = 1$ unless noted otherwise.

For a vertically isothermal disk in hydrostatic balance (with no self-gravity), the mid-plane pressure of disk gas is

$$P_\mathrm{d} = 6.9 \times 10^{-3} F_\Sigma \sqrt{F_T}\, a_{10}^{-45/14}\ \mathrm{dyn\ cm^{-2}} \tag{2}$$

for a molecular weight of $\mu = 2.35$ proton masses and a Solar mass star.

The (thermodynamically isothermal) sound speed in the disk is

$$c_\mathrm{d} = \sqrt{\mathcal{R} T_\mathrm{d}} = 0.4 \sqrt{F_T} a_{10}^{3/14}\ \mathrm{km\ s^{-1}} \tag{3}$$

in terms of the specific gas constant $\mathcal{R}$. The disk scale height is

$$H_\mathrm{d} = c_\mathrm{d}/\Omega = 0.42 \sqrt{F_T}\, a_{10}^{9/7}\ \mathrm{AU}\,. \tag{4}$$

in terms of the Keplerian frequency $\Omega = \sqrt{GM_*/a^3}$, with G the gravitational constant and M_* the stellar (in this work Solar) mass.

We assume a dust opacity following Bell & Lin (1994):

$$\kappa = 2F_\kappa \left(\frac{T}{100\text{ K}}\right)^\beta \text{ cm}^2\text{ g}^{-1}, \quad (5)$$

with a powerlaw index $\beta = 2$ and normalization $F_\kappa = 1$ unless noted otherwise. Grain growth tends to lower both F_κ and β, while dust abundance scales with F_κ. Section §6.2 discusses dust sublimation and more realistic opacity laws.

2.2. *Length Scales*

The characteristic length scales for protoplanetary atmospheres are crucial for choosing boundary conditions and for understanding the validity of spherical symmetry in a disk of scale height H_d. The radius of the solid core is

$$R_\text{c} \equiv \left(\frac{3M_\text{c}}{4\pi\rho_\text{c}}\right)^{1/3} \approx 10^{-4} m_\text{c10}^{1/3} \text{ AU}, \quad (6)$$

where the core mass, M_c, is normalized to 10 Earth masses as $m_\text{c10} \equiv M_\text{c}/(10\ M_\oplus)$. The core density is held fixed at $\rho_\text{c} = 3.2$ g cm^{-3}. We thus neglect the detailed equation of state of the solid core (Fortney et al. 2007).

A planet can bind a dense atmosphere if its escape velocity exceeds the sound speed. This criterion is satisfied inside the Bondi radius

$$R_\text{B} \equiv \frac{GM_\text{p}}{c_\text{d}^2} \approx 0.17 \frac{m_\text{p10}\, a_{10}^{3/7}}{F_T} \text{ AU} \quad (7)$$

where the enclosed planet mass, $M_\text{p} = M_\text{c} + M_\text{atm}$, includes the core and any atmosphere within the Bondi radius. The scalings thus use $m_\text{p10} \equiv M_\text{p}/(10\ M_\oplus)$.

Stellar tides dominate the planet's gravity beyond the Hill radius

$$R_\text{H} = \left(\frac{M_\text{p}}{3M_*}\right)^{1/3} a \approx 0.22\, m_\text{p10}^{1/3}\, a_{10} \text{ AU}, \quad (8)$$

where hydrostatic balance breaks down. In Equation (8), M_p includes mass enclosed within R_H. During the early stages of evolution, $M_\text{p} \sim M_\text{c}$, and the core mass can be used to get estimates of both R_B and R_H.

The relevant length scales of the atmosphere and disk satisfy the relation $R_\text{B} H_\text{d}^2 = 3R_\text{H}^3$. The length scales are roughly equal at the "thermal mass" (e.g., Menou & Goodman 2004)

$$M_\text{th} > \frac{c_\text{d}^3}{G\Omega} \approx 25 \frac{F_T^{3/2}}{\sqrt{m_*}} a_{10}^{6/7}\ M_\oplus\,. \quad (9)$$

In the low mass regime, $M_\text{p} < M_\text{th}/\sqrt{3}$, the length scales order as $R_\text{B} < R_\text{H} < H_\text{d}$ (Rafikov 2006, hereafter R06). In this regime, many studies assume the atmosphere matches the disk conditions at R_B. We, however, use R_H as the matching radius in both this low mass and other higher mass regimes. This choice is justified by the fact that, for hydrostatic solutions, the density at R_B exceeds the disk's background density by an order unity factor (R06). Nevertheless, since the density change is modest, the choice of outer boundary condition has a similarly modest effect on our results.

For a finite range of intermediate masses, $M_\text{th}/\sqrt{3} < M_\text{p} < 3M_\text{th}$, the Hill radius is the smallest scale, satisfying both $R_\text{H} < R_\text{B}$ and $R_\text{H} < H_\text{d}$. Spherical symmetry remains a good, if imperfect, approximation because the disk is only weakly vertically stratified on scales $\lesssim H_\text{d}$.

At higher planet masses where $M_\text{p} > 3M_\text{th}$ and $H_\text{d} < R_\text{H} < R_\text{B}$, spherical symmetry is no longer a good approximation, due to both the vertical stratification of the disk and gap opening. See §6.1 for discussion of neglected non-hydrostatic effects on all mass scales.

Note that while R_H is the outer boundary of our structure calculations, we define planet masses to include only the mass inside the smaller of R_B or R_H. This conservative choice in quoting planet masses is usually a minor distinction because (when $R_\text{B} < R_\text{H}$) the gas between R_B and R_H is weakly compressed.

2.3. *Structure Equations and Boundary Conditions*

Our atmosphere calculations use the standard structure equations of mass conservation, hydrostatic balance, thermal gradients, and energy conservation:

$$\frac{dm}{dr} = 4\pi r^2 \rho \quad (10a)$$

$$\frac{dP}{dr} = -\frac{Gm}{r^2}\rho \quad (10b)$$

$$\frac{dT}{dr} = \nabla \frac{T}{P}\frac{dP}{dr} \quad (10c)$$

$$\frac{dL}{dr} = 4\pi r^2 \rho \left(\epsilon - T\frac{\partial S}{\partial t}\bigg|_m\right), \quad (10d)$$

where r is the radial coordinate, and P, T, ρ and L are the gas pressure, temperature, density and luminosity, respectively. The enclosed mass at radius r is m. Equation (10c) simply defines the temperature gradient $\nabla \equiv d\ln T/d\ln P$. In optically thick radiative zones, radiative diffusion gives a temperature gradient

$$\nabla_\text{rad} \equiv \frac{3\kappa P}{64\pi G m \sigma T^4} L, \quad (11)$$

where σ is the Stefan-Boltzmann constant. In our models the atmosphere is optically thick throughout the whole radiative region (see Appendix B.3 for an analytic estimate of the optical depth). In convectively unstable regions, efficient convection gives an isentropic temperature gradient with $\nabla = \nabla_\text{ad}$, the adiabatic gradient

$$\nabla_\text{ad} \equiv \left(\frac{d\ln T}{d\ln P}\right)_\text{ad}. \quad (12)$$

According to the Schwarzschild criterion, convective instability occurs when $\nabla_\text{rad} > \nabla_\text{ad}$. Thus $\nabla = \min(\nabla_\text{rad}, \nabla_\text{ad})$ sets the temperature gradient.

In the energy equation (10d), ϵ represents all local sources of heat input, which excludes the motion of the atmosphere itself. In stars, nuclear burning contributes to ϵ. In a protoplanetary atmosphere, dissipative drag on planetesimals contributes to ϵ. Our simplified models set $\epsilon = 0$, consistent with our neglect of planetesimal accretion luminosity at the base of the atmosphere.

The $\epsilon_g = -T\partial S/\partial t$ term gives the energy input from gravitational contraction.[1] The partial time derivative would normally require our radial derivatives to be partial derivatives. However, our subsequent developments will replace the local energy equation (10d) with global energy balance (see section §2.4), reverting the structure equations to time-independent ordinary differential equations (ODEs).

To solve the equation set (10), an EOS is required for closure. In our study, we adopt an ideal gas law with a polytropic EOS

$$P = \rho \mathcal{R} T \,, \tag{13a}$$
$$P = K \rho^{\gamma} \,, \tag{13b}$$

where K is the adiabatic constant. The adiabatic index is $\gamma = 1/(1 - \nabla_{\rm ad})$. This work uses $\nabla_{\rm ad} = 2/7$ for an ideal diatomic gas (by comparison, an ideal monatomic gas has $\nabla_{\rm ad} = 2/5$). While our reference mean molecular weight ($\mu = 2.35$ proton masses) includes Helium, we ignore Helium's effect on the EOS, which is already greatly simplified. The second law or thermodynamics gives the relative entropy as

$$S = \mathcal{R} \ln \left(\frac{T^{1/\nabla_{\rm ad}}}{P} \right) , \tag{14}$$

eliminating the need for K.

Boundary conditions must be satisfied at both the base and the top of the atmosphere with $m(R_{\rm c}) = M_{\rm c}$, $T(R_{\rm H}) = T_{\rm d}$ and $P(R_{\rm H}) = P_{\rm d}$. In principle, our solutions describe atmospheres with $L(R_{\rm c}) = 0$. In practice, since we do not directly integrate Equation (10d) we need not directly impose this boundary condition, as described in §2.5.

2.4. *Global Cooling of an Embedded Planet*

This section describes the global energy balance of a planet embedded in a gas disk, or more generally any spherical, hydrostatic object in pressure equilibrium with a background medium. The total atmospheric energy includes gravitational and internal energies, $E = E_G + U$, with

$$E_G = -\int_{M_{\rm c}}^{M} \frac{Gm}{r} dm \,, \tag{15a}$$
$$U = \int_{M_{\rm c}}^{M} u dm \,. \tag{15b}$$

The specific internal energy is $u = C_V T = \mathcal{R}(\nabla_{\rm ad}^{-1} - 1)T$ for a polytropic EOS. For a star or coreless planet, $M_{\rm c} = 0$.

We start with the global energy balance for an isolated planet of mass M with a free surface:

$$L_M = L_{\rm c} + \Gamma - \dot{E}. \tag{16}$$

The surface luminosity, L_M, includes contributions from the core luminosity $L_{\rm c}$ – e.g. planetesimal accretion or radioactive decay – from the total heat generation Γ – given by the integral of ϵ over the object – and from the rate of change of atmospheric energy $\dot{E}$, a loss term.

[1] In general, any motion is accounted for by this term. The partial time derivative is performed on shells of fixed mass.

For an object with no core luminosity (or no core) and no internal heat sources, the energy equation $L_M = -\dot{E}$ describes KH contraction in its simplest form. When internal heat sources dominate, $L_M = \Gamma$, e.g. for nuclear burning in an main sequence star.

A protoplanetary atmosphere embedded in a gas disk lacks a free surface. For objects without a free surface (or interior to a free surface), the full energy equation,

$$L_M = L_{\rm c} + \Gamma - \dot{E} + e_M \dot{M} - P_M \left. \frac{\partial V_M}{\partial t} \right|_M , \tag{17}$$

acquires surface terms as derived in Appendix A. The surface can be at any mass level M, where the instantaneous radius is R. Other surface quantities are labeled by M subscripts. The energy accreted across the surface is given by the specific energy, $e_M = u_M - GM/R$, and the mass accretion rate of gas, $\dot{M}$. The work done by the surface is $P_M \partial V_M/\partial t$, with the partial derivative performed at fixed mass.

For static solutions, which are not the focus of this paper, the surface terms (and also $\dot{E}$) vanish. Static solutions are valid when imposed heat sources, i.e. $L_{\rm c}$ and Γ, exceed the atmospheric losses. Quantitatively, static solutions apply when the KH timescale,

$$\tau_{\rm KH} \sim \frac{|E|}{L_M}, \tag{18}$$

is shorter than the actual evolutionary timescale. Thus, $\tau_{\rm KH}$, which our models calculate, gives strong lower limits on the time to form giant planets by core accretion.

2.5. *The Two-Layer Model*

To simplify our calculations of atmospheric contraction we use a two-layer model with a bottom convective region and an upper radiative layer. The existence of such a structure is well known from previous studies (e.g., R06) and can be readily understood. Before the protoplanetary atmosphere can cool, it has the entropy of the disk. As the atmosphere cools, the deep interior remains convective. Convective interiors are a common feature of low mass cool objects (brown dwarfs and planets) that results from the behavior of $\nabla_{\rm rad}$ for realistic opacity laws. However, the entropy of the deep interior decreases as the atmosphere cools. A region of outwardly increasing entropy, i.e. a radiative layer, is required to connect the convective interior to the disk. A more complicated structure, with radiative windows in the convection zone, is possible as discussed in §6.2.

In convective regions, the adiabatic structure is independent of luminosity and can be calculated without local energy balance, Equation (10d). Thus, for fully convective objects, a cooling sequence can be established by connecting a series of adiabatic solutions using a global energy equation, $L_M = -\dot{E}$ or Equation (16). Such methods are commonly used for their computational efficiency and are sometime referred to as "following the adiabats," since the steady state solutions evolve in order of decreasing entropy (Marleau & Cumming 2013).

In the radiative zone, local energy balance, Equation (10d), does affect the atmospheric structure. We proceed by assuming that the majority of energy is lost from the convective interior, and thus the luminosity

can be treated as constant in the outer radiative zone. With this approximation we can construct solutions from Equations (10a – c) that "follow the mass," i.e. gradually increase the atmospheric mass. We then use global energy balance, Equation (17), to place these solutions in a cooling sequence. The validity of neglecting luminosity generation in the radiative zone can be checked *a posteriori*.

To obtain a single atmosphere profile (indexed by i), we choose a planet mass M_i. At the outer boundary, at $R_{\rm H}(M_i)$, the temperature and pressure are set to the disk values. To integrate Equations (10a–c), the luminosity is required to compute $\nabla_{\rm rad}$. The correct value of the luminosity is not known in advance, and is the eigenvalue of the problem. The boundary conditions can only be satisfied for the correct value of the luminosity eigenvalue, which we find by the shooting method. Specifically, we alter the luminosity until the integrated value of mass at the core, $m(R_{\rm c})$, matches the actual core mass, $M_{\rm c}$.

To establish the time difference between neighboring solutions, we apply Equation (17) at the radiative-convective boundary (RCB) of the solutions. In principle, energy balance could be evaluated at any level. Our approximate treatment of the radiative zone makes the RCB the preferred location. With $\Gamma = L_{\rm c} = 0$, the elapsed time Δt between states i and $i+1$ is given by the finite difference

$$\Delta t = \frac{-\Delta E + \langle e \rangle \Delta M - \langle P \rangle \Delta V_{\langle M \rangle}}{\langle L \rangle} \,. \tag{19}$$

Brackets indicate an average of, and "Δ" indicates a difference between, the two states. All values are evaluated at the RCB. Due to the partial derivative in Equation (17), the volume difference $\Delta V_{<M>}$ is performed at fixed mass, here the average of the masses at the RCB.

3. ANALYTIC COOLING MODEL

This section develops the analytic version of our two-layer model, which is useful for predicting and explaining the results of numerical evolution models. To obtain our analytic results, we neglect self-gravity. As shown in §4, self-gravity becomes quantitatively important at surprisingly low atmospheric masses, $M_{\rm atm} \gtrsim 0.2 M_{\rm c}$. Thus the analytic model cannot accurately model the later stages of evolution. Nevertheless, this model does explain general trends, including the dependence on opacity and disk temperature and pressure.

The analytic model also assumes that the upper radiative radiative layer is thick, with a pressure depth $P_{\rm RCB} \gg P_{\rm d}$. This approximation limits the ability to study the initial cooling of very low mass atmospheres with thin outer radiative zones. However, since early evolution is quite rapid, this approximation negligibly affects total cooling times and critical core masses, our main foci.

3.1. *Two Layer Structure*

To apply the two-layer cooling model analytically, we require expressions for the atmospheric structure. Conditions at the RCB are crucial as they set the interior adiabat and the radiative losses. (Recall that luminosity generation in the radiative zone is neglected.) We express the temperature and pressure of the RCB, at the radius $R_{\rm RCB}$, as

$$T_{\rm RCB} = \chi T_{\rm d} \tag{20a}$$

$$P_{\rm RCB} = \theta P_{\rm d} e^{R_{\rm B}/R_{\rm RCB}} \,. \tag{20b}$$

The leading constants would be unity, $\chi = \theta = 1$, if the radiative zone were replaced by an isothermal layer. In practice, deviations from unity are modest. Standard radiative structure calculations (see Appendix B.2 for details) give

$$\chi \simeq \left(1 - \frac{\nabla_{\rm ad}}{\nabla_\infty}\right)^{-\frac{1}{4-\beta}} \simeq 1.53 \,, \tag{21}$$

for $P_{\rm RCB} \gg P_{\rm d}$, our regime of interest, and with the radiative temperature gradient at infinite depth, $\nabla_\infty = 1/2$, for our dust opacity. The radiative zones are thus nearly isothermal, as also found by R06. While a simple closed form expression is not possible, the factor $\theta \simeq 0.556$ for our parameters.

Given the conditions at the RCB, the density and temperature profiles along the interior adiabat,

$$\rho = \rho_{\rm RCB} \left[1 + \frac{R'_{\rm B}}{r} - \frac{R'_{\rm B}}{R_{\rm RCB}}\right]^{1/(\gamma-1)} \tag{22a}$$

$$T = T_{\rm RCB} \left[1 + \frac{R'_{\rm B}}{r} - \frac{R'_{\rm B}}{R_{\rm RCB}}\right] \,, \tag{22b}$$

follow from hydrostatic balance. We introduce an effective Bondi radius

$$R'_{\rm B} \equiv \frac{G M_{\rm c}}{C_P T_{\rm RCB}} = \frac{\nabla_{\rm ad}}{\chi} R_{\rm B} \tag{23}$$

to simplify expressions, with $C_P = \mathcal{R}/\nabla_{\rm ad}$ the specific heat at constant pressure.

Deep in the adiabatic interior, where $r \ll R_{\rm RCB} \ll R'_{\rm B}$, the profiles follow simple power laws,

$$\rho \simeq \rho_{\rm RCB} \left[\frac{R'_{\rm B}}{r}\right]^{1/(\gamma-1)} \propto r^{-5/2} \tag{24a}$$

$$T \simeq T_{\rm RCB} \frac{R'_{\rm B}}{r} = \frac{G M_{\rm c}}{C_P r} \,. \tag{24b}$$

While the radial density profile depends on the adiabatic index, the r^{-1} temperature scaling is universal. For reference, if self-gravity is included, the temperature profile satisfies

$$\frac{dT}{dr} = -\frac{G m(r)}{C_P r^2} \,. \tag{25}$$

Thus, the enclosed mass gives a temperature profile flatter than $T \propto r^{-1}$ in self-gravitating models.

Returning to our non-self-gravitating model, the total specific energy at depth,

$$e = e_g + u = -\nabla_{\rm ad} \frac{G M_{\rm c}}{r} \,, \tag{26}$$

is simply proportional to the gravitational potential, $e_g = -G M_{\rm c}/r$.

3.2. *Mass, Energy and Luminosity*

The most relevant quantities for global cooling are the integrated energy, luminosity, and atmospheric mass. In our non-self-gravitating limit, the mass of our nearly

isothermal radiative zones is less than the convective interior, as shown in Appendix B.1.

The atmospheric mass is thus given by the integration of Equation (22a),

$$M_{\rm atm} = \frac{5\pi^2}{4}\rho_{\rm RCB} {R'_{\rm B}}^{5/2}\sqrt{R_{\rm RCB}}, \tag{27}$$

in the relevant limit $R_{\rm c} \ll R_{\rm RCB} \ll R'_{\rm B}$ and for $\gamma = 7/5$. Mass is concentrated near the outer regions of the convective zone, a result that holds for $\gamma > 4/3$.

Using Equation (20b) to eliminate $R_{\rm RCB}$, the critical ratio of atmosphere to core mass becomes

$$\frac{M_{\rm atm}}{M_{\rm c}} = \frac{P_{\rm RCB}}{\xi P_M}, \tag{28}$$

where we define a characteristic pressure and a logarithmic factor

$$P_M \equiv \frac{4\nabla_{\rm ad}^{3/2}}{5\pi^2\sqrt{\chi}}\frac{GM_{\rm c}^2}{{R'_{\rm B}}^4} \tag{29a}$$

$$\xi \equiv \sqrt{\ln[P_{\rm RCB}/(\theta P_{\rm d})]}\,. \tag{29b}$$

The atmosphere mass increases as radiative losses lower the internal adiabat and increase $P_{\rm RCB}$. The crossover mass, $M_{\rm atm} = M_{\rm c}$, is reached when

$$P_{\rm RCB} = \xi P_M, \tag{30}$$

i.e. near the characteristic pressure P_M. The critical value of the order unity factor ξ is found by eliminating $P_{\rm RCB}$ from Equations (29b) and (30). This logarithmic factor complicates our analytic description, but since it remains order unity we simply hold it fixed in our scalings.

The total energy is concentrated towards the core if $|u|\rho r^3 \propto \rho r^2$ drops with increasing r. This condition requires $\gamma < 3/2$, which our choice of $\gamma = 7/5$ satisfies, but $\gamma = 5/3$ (monatomic gas) would not. Integration of Equation (26) over the mass of the atmosphere thus gives

$$E = -4\pi\nabla_{\rm ad} G M_{\rm c}\int_{R_{\rm c}}^{R_{\rm RCB}} \rho r dr \tag{31a}$$

$$\approx -4\pi P_{\rm RCB} {R'_{\rm B}}^{\frac{1}{\nabla_{\rm ad}}}\left(\frac{\gamma-1}{3-2\gamma}\right) R_{\rm c}^{\frac{2\gamma-3}{\gamma-1}} \tag{31b}$$

$$\approx -8\pi P_{\rm RCB}\frac{{R'_{\rm B}}^{7/2}}{\sqrt{R_{\rm c}}} \tag{31c}$$

with $\gamma < 3/2$ and $\gamma = 7/5$ in Equations (31b) and (31c), respectively.

The emergent luminosity from the RCB,

$$L_{\rm RCB} = \frac{64\pi G M_{\rm RCB}\sigma T_{\rm RCB}^4}{3\kappa P_{\rm RCB}}\nabla_{\rm ad} \approx L_{\rm d}\frac{P_{\rm d}}{P_{\rm RCB}}\,, \tag{32}$$

follows from Equation (11) and marginal convective stability, $\nabla_{\rm rad} = \nabla_{\rm ad}$, where we define

$$L_{\rm d} \equiv \frac{64\pi G M_{\rm RCB}\sigma T_{\rm d}^4}{3\kappa(T_{\rm d})P_{\rm d}}\nabla_{\rm ad}\chi^{4-\beta}. \tag{33}$$

The inverse scaling $L_{\rm RCB} \propto 1/P_{\rm RCB}$ shows that luminosity drops as the atmosphere cools and $P_{\rm RCB}$ deepens. This result relies on the pressure independence of dust opacities. For fully non-self-gravitating results, we replace $M_{\rm RCB}$, the mass up to the RCB, with the core mass, but the mass of the convective atmosphere can be included for a slightly higher order estimate.

3.3. *Cooling Times & Core Masses*

Our analytic cooling model uses $L = -\dot{E}$, neglecting the surface terms in Equation (17).[2] Applying Equations (31c) and (32), the time it takes to cool the atmosphere until the RCB reaches a given pressure depth, $P_{\rm RCB}$, is

$$t_{\rm cool} = -\int_{P_{\rm d}}^{P_{\rm RCB}}\frac{dE/dP_{\rm RCB}}{L_{\rm RCB}}dP_{\rm RCB} \tag{34a}$$

$$\approx 4\pi\frac{P_{\rm RCB}^2}{P_{\rm d}}\frac{{R'_{\rm B}}^{7/2}}{L_{\rm d}\sqrt{R_{\rm c}}}\,. \tag{34b}$$

The initial RCB depth, set to $P_{\rm d}$ as a formality, is of little importance because the cooling slows as it proceeds with $t_{\rm cool} \propto P_{\rm RCB}^2$.

The most relevant cooling time is the crossover time, $t_{\rm co}$, required to reach the crossover mass, $M_{\rm atm} = M_{\rm c}$. Equations (34) and (30) give this time as

$$t_{\rm co} \approx 2\times10^8\frac{F_T^{5/2}F_\kappa\left(\frac{\xi}{3.4}\right)^2}{m_{\rm c10}^{5/3}a_{10}^{15/14}}\ {\rm yr}\,. \tag{35}$$

The corresponding critical core mass, $M_{\rm crit}$, has a crossover time that equals the typical lifetime of a protoplanetary disk

$$t_{\rm d} = 3\times10^6\ {\rm yr}\,. \tag{36}$$

Setting $t_{\rm co} = t_{\rm d}$ gives

$$M_{\rm crit} \approx 100\frac{F_T^{3/2}F_\kappa^{3/5}\left(\frac{\xi}{2.6}\right)^{6/5}}{a_{10}^{9/14}}\ M_\oplus. \tag{37}$$

Both $t_{\rm co}$ and $M_{\rm crit}$ are too large to be interesting, or to be correct based on previous results and the numerical results in this paper. The main reason for this discrepancy is the neglect of self-gravity, as shown in Section 4. The magnitude of the discrepancy may be surprising as one might expect self-gravity to be a modest factor for $M_{\rm atm} \leq M_{\rm c}$. Clearly this seemingly reasonable expectation can be misleading, an interesting result in itself.

Aside from this insight, the analytic model is useful because, despite the amplitude error, it explains the basic scaling of numerical cooling models. As is well known, a lower opacity, here scaling with F_κ, accelerates growth and gives a lower critical core mass. Lower disk temperatures also decrease both $t_{\rm co}$ and $M_{\rm crit}$. Furthermore, the decline in both quantities with semimajor axis is completely generated by the disk temperature law (ignoring the logarithmic ξ). The temperature dependence is a competition between two main effects. The higher luminosity, $\propto T^{4-\beta}$, at higher temperatures gives faster cooling, which opposes the overall effect. The larger Bondi radius, and the effectively stronger gravity of the core, is the dominant effect that gives faster cooling at lower

[2] Appendix B.4 shows that these terms are negligible for a non-self-gravitating model, but they do become relevant when self-gravity is important and included.

temperatures. For different β values, $t_{\rm co} \propto F_T^{\beta+1/2}$, so the slope of the dust opacity is an important moderating effect on the cooling.

The cooling timescale and critical core mass depend only weakly on the disk pressure, via the logarithmic factor ξ. Section §5.1 shows that these analytic predictions for disk temperature and pressure dependence compare favorably with numerical results. Moreover, the analytic estimates quantitatively reproduce the numerical results to reasonable accuracy, if the effective crossover mass for unstable atmosphere collapse is a fraction of the core mass, i.e. $M_{\rm atm} = f M_{\rm c}$. Under this assumption, Equations (35) and (37) become

$$t_{\rm co} \approx 2 \times 10^8 \frac{F_T^{5/2} F_\kappa \left(\frac{\xi}{3.4}\right)^2 f^2}{m_{\rm c10}^{5/3} a_{10}^{15/14}} \ {\rm yr} \tag{38}$$

$$\approx 3 \times 10^6 \frac{F_T^{5/2} F_\kappa \left(\frac{\xi}{3.4}\right)^2}{m_{\rm c10}^{5/3} a_{10}^{15/14}} \ {\rm yr} \tag{39}$$

and

$$M_{\rm crit} \approx 100 \frac{F_T^{3/2} F_\kappa^{3/5} \left(\frac{\xi}{2.6}\right)^{6/5} f^{6/5}}{a_{10}^{9/14}} \ M_\oplus \tag{40}$$

$$\approx 8 \frac{F_T^{3/2} F_\kappa^{3/5} \left(\frac{\xi}{2.6}\right)^{6/5}}{a_{10}^{9/14}} \ M_\oplus \ , \tag{41}$$

with $f = 0.13$ in Equations (39) and (41). We choose this particular fractional scaling to match our numerical results at 10 AU (see section §5 for more details). We note that the scaling above is valid if the logarithmic factor ξ is fixed; however, the analytic estimates presented in section §5 explicitly take into account the dependence of ξ on the core mass (see Equations 29b and 30).

4. QUASI-STATIC KELVIN-HELMHOLTZ CONTRACTION

We now present some representative examples of the structure and evolution of our model atmospheres, calculated as described in §2, with some comparisons made to the non-self-gravitating analytic model of §3. Radial structure is presented in §4.1, time evolution is described in §4.2, and the regimes of validity of our two-layer cooling model are examined in §4.3.

4.1. *Atmospheric Stucture*

Figure 1 shows radial profiles at different stages of atmospheric growth. In these examples, we fix the core mass at $M_{\rm c} = 5 M_\oplus$ and the radial disk location to $a = 60$ AU. The quoted mass values include the core plus atmosphere within the smaller of $R_{\rm B}$ or $R_{\rm H}$, which for these cases is $R_{\rm B}$. The 9.24 $M_\oplus$ solution is the highest mass we can reach in our evolutionary sequence, as we explain further in §4.3.

The lowest mass atmosphere – which we take as our initial state – is fully convective with the same entropy as the disk. In Fig. 1 this state is the 5.01 $M_\oplus$ solution with no radiative zone. Atmospheric cooling and contraction allows the accretion of more gas. In the convective zones, higher mass solutions contain lower entropy and higher pressures. A radiative zone emerges to connect the lower entropy interior to the higher entropy disk. Fig. 1 shows that this radiative zone is already fairly deep in the 5.10 $M_\oplus$ solution.

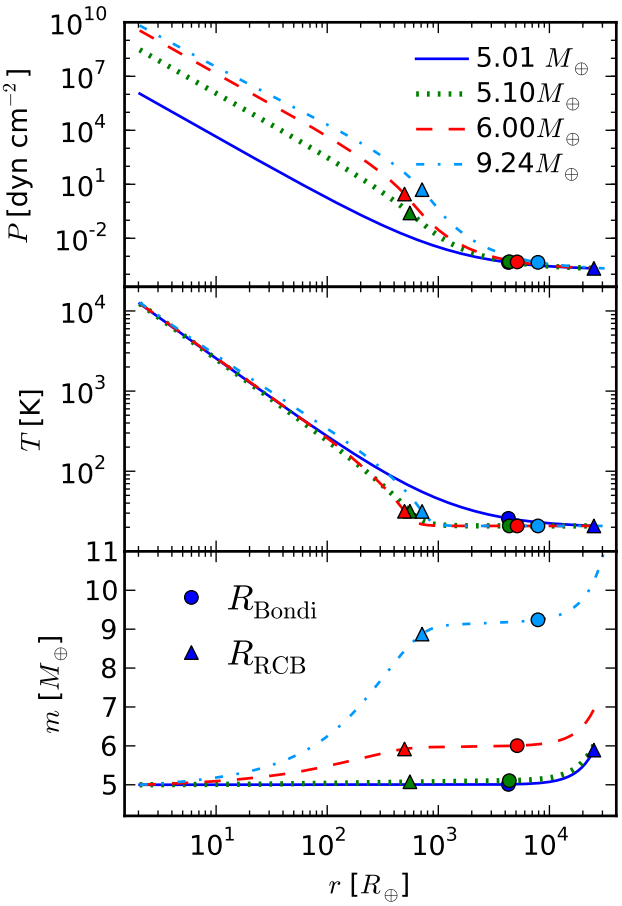

FIG. 1.— Radial profiles of atmospheric pressure, temperature and enclosed mass (including the core) for a $5 M_\oplus$ core at $a = 60$ AU. Solid, dotted, dashed and dot-dashed lines correspond to solutions with total mass (core and atmosphere) of $5.01 M_\oplus$, $5.10 M_\oplus$, $6.00 M_\oplus$ and $9.24 M_\oplus$, respectively. (See text for a description of evolution to yet higher masses.) Circles and triangles mark the locations of the Bondi radii and of the radiative-convective boundaries, respectively. The radial profiles extend from the core to the Hill radius.

The detailed structure of these profiles is well approximated by our non-self-gravitating, analytic solutions. Deep in convective zones, Equation (24) gives that $T \propto r^{-1}$ and $P \propto r^{-1/\nabla_{\rm ad}}$. This behavior is seen in the low mass solutions in Fig. 1. As explained by Equation (25), the high mass solutions show a slightly flatter profile in T and also in $P \propto T^{1/\nabla_{\rm ad}}$. In agreement with Equation (20), the radiative zones remain nearly isothermal, even for the higher masses. Consequently, the pressure increases nearly exponentially with inverse depth.

4.2. *Time Evolution*

The cooling model of §2.5 is used to connect solutions of different atmospheric masses into an evolutionary sequence. Fig. 2 shows the luminosity evolution and the

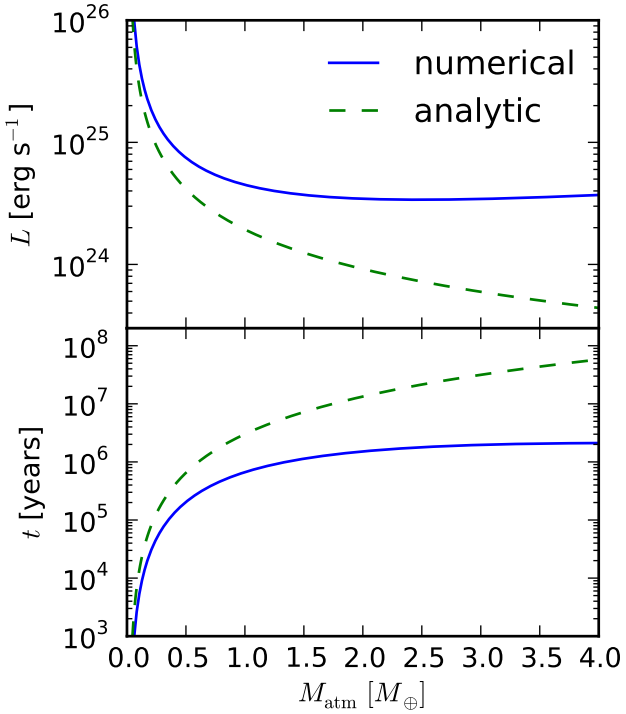

FIG. 2.— Evolution of the luminosity and elapsed time during atmospheric growth around a $5M_\oplus$ core at 60 AU. The luminosity is initially high, then decreases as the atmosphere grows in mass and the radiative zone becomes optically thicker. Due to the neglect of self-gravity, the analytic model (*dashed curve*) gives a further drop in luminosity and a longer evolution time.

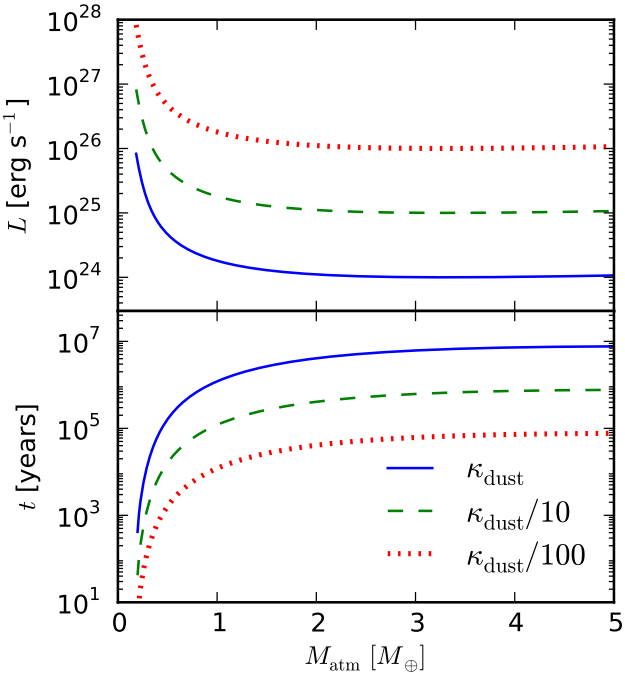

FIG. 3.— Similar to Fig. 2, but for a $5M_\oplus$ core forming at 10 AU; we show the effect of reducing the dust abundance by factors of 10 and 100 from standard Solar abundances. The reduced dust opacities give higher luminosities and faster atmospheric growth.

elapsed time as a function of atmospheric mass for a $5M_\oplus$ core at 60 AU, i.e. the same parameters as in Fig. 1. During the early stages of atmospheric growth, the luminosity drops sharply. This behavior is seen in both the full numerical solutions (with solid lines) and the analytic model (with dashed lines). The increasing pressure depth of the RCB with mass causes increases in the optical depth ($\propto \kappa P$) and decreases in the radiative luminosity. This behavior is described in Equations (28) and (32).

At later stages of evolution, the numerical model in Fig. 2 shows a flat luminosity with increasing mass and also time (not shown). By contrast, the non-self-gravitating analytic model gives a luminosity that continues to drop with increasing mass. To understand this difference, we note that the scaling of Equation (32), $L_{\rm RCB} \propto M_{\rm RCB} T_{\rm RCB}^4/(\kappa_{\rm RCB} P_{\rm RCB})$, holds in both cases; thus accounting for the higher enclosed mass in the self-gravitating model gives a somewhat higher luminosity, as desired. However, the main effect is that Equation (28) – which describes a nearly linear relation between atmospheric mass and RCB pressure – breaks down for self-gravitating solutions. This behavior can be seen in the top panel of Fig. 1 where the $P_{\rm RCB}$ increases significantly from 5.10 to 6.0 $M_\oplus$, but only increases relatively modestly with further growth to 9.24 $M_\oplus$. To allow these relatively lower $P_{\rm RCB}$ values (and thus higher luminosities) in the higher mass solutions, the radius $R_{\rm RCB}$ must shift outwards, as shown in Fig. 1.

The accelerated growth in the numerical model, as shown in the bottom panel of Fig. 2, is also a direct result of the enhanced cooling (higher luminosities) in the self-gravitating models. We see that self-gravity plays a very important role in atmospheric evolution, even well before the crossover mass.

In Fig. 3, the opacity normalization in Equation (5) is reduced by factors of 10 and 100. Lower opacities result in higher luminosities and faster evolution. Our model thus confirms this well-established result (Hubickyj et al. 2005). While clearly an important effect, atmospheric dust opacities are difficult to robustly predict. Ablation of infalling solids is a dust source. Sinks include the sequestration of solids in the core and dust settling through the radiative zone. Grain growth both reduces dust opacities per unit mass and favors settling. Our scenario of negligible ongoing particle accretion tends to favor low dust opacities. To be conservative, however, our reference case considers full Solar abundances. The effect of opacity reduction on the critical core mass is described in §5.

Fig. 4 plots the evolution of the atmospheric growth timescale, $M_{\rm atm}/\dot{M}$, around a $5M_\oplus$ core at several locations in our reference disk model. This instantaneous growth time shows clearly that the atmosphere spends the bulk of its time growing though intermediate atmospheric masses, $\sim 1-3\ M_\oplus$ in this case. Growth times are short both early – when the radiative zone is relatively transparent – and late – when self-gravity accelerates growth. The accelerated growth at higher masses is also evident in Figs. 2 and 3 (bottom panels) as the flattening of the t vs. $M_{\rm atm}$ curve.

The fact that growth times peak before the crossover mass, when $M_{\rm atm} < M_{\rm c}$, is helpful for understanding

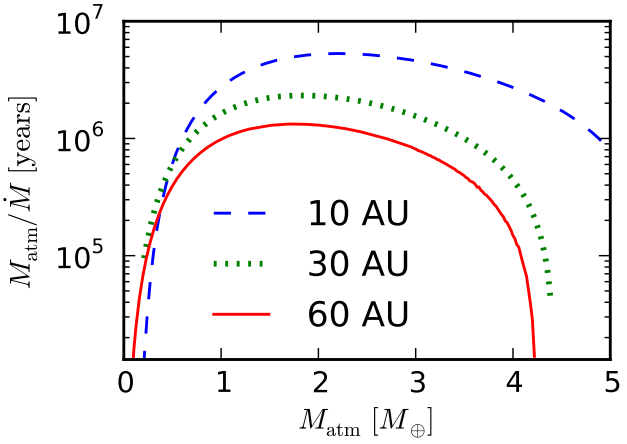

FIG. 4.— Evolution of the atmospheric growth timescale with mass around a $5M_\oplus$ solid core located at 10, 30 or 60 AU. Growth is slowest for $M_{\rm atm} \sim 1-3M_\oplus$, i.e. before the crossover mass at $M_{\rm atm} = M_{\rm c}$.

atmospheric growth. The estimated timescale to runaway growth can be well approximated by only considering the time it takes to grow to the crossover mass, or even to a somewhat lower mass. This insensitivity to the upper mass threshold is characteristic of accelerating growth. We next show how this behavior is fortuitous, as our model assumptions can break down during the later stages of atmospheric growth.

4.3. *Validity of the Two-Layer Cooling Model*

To examine the regimes where our cooling model is valid, we compare the model luminosity to the additional neglected luminosity, $L_{\rm negl}$, that a more detailed model would have generated in the radiative zone. To compute $L_{\rm negl}$ we compute the entropy difference between successive radiative zone solutions. We then integrate the energy equation, $\partial L/\partial m = -T\partial S/\partial t$, over the average depth of the radiative zone.[3]

Fig. 5 shows that the neglected luminosity is indeed negligible during the early stages of evolution. However, $L_{\rm negl}$ exceeds the model luminosity, L, at high masses, $M_{\rm atm} > 3M_\oplus$ in this case, meaning that our model becomes inaccurate at late states. Nevertheless, our cooling model gives reasonably reliable estimates of core accretion timescales. As shown above, the growth time is mostly spent at low masses, when $L_{\rm negl}$ is small and safely neglected.

The (non-vanishing) individual terms in the global cooling model of Equation (17), evaluated at the RCB, are also plotted in Fig. 5. At low masses, the change in energy, $-\dot{E}$, makes the dominant contribution to luminosity. As the mass increases, the surface terms become more significant, led by the accretion energy. However the surface terms are everywhere smaller than $L_{\rm negl}$. Thus wherever our model is accurate – including the crucial early phases of growth – surface terms are a minor correction.

[3] While useful as a diagnostic, the neglected luminosity cannot reliably correct the global cooling model because the effects of $L_{\rm negl}$ on the structure of the radiative zone are still ignored.

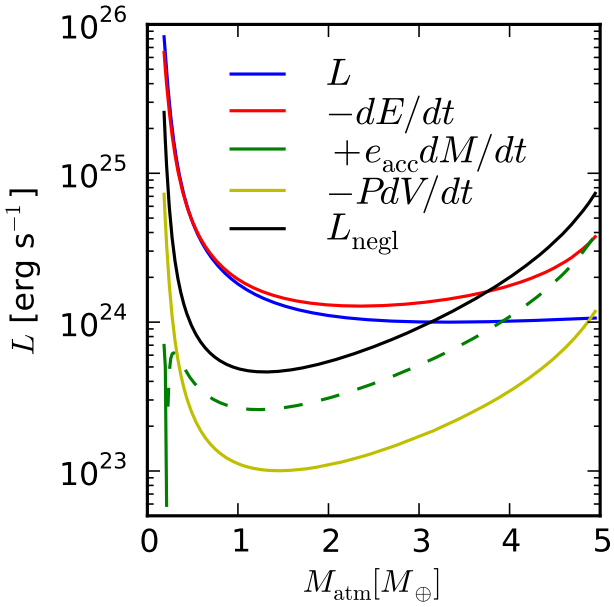

FIG. 5.— Individual terms in the atmospheric cooling model of Equation (17), for a $5M_\oplus$ core at 10 AU. The dashed curve for accretion energy indicates a negative contribution. All quantities are evaluated at the RCB, except for $L_{\rm negl}$, the extra luminosity that would have been generated in the radiative zone, but is neglected in our model. The neglected luminosity is a small correction to the model luminosity L for $M_{\rm atm} \lesssim 3M_\oplus$. Since these low masses dominate growth times, our model is roughly accurate.

At yet higher masses than shown in Fig. 5, our cooling model breaks down. Mathematically, the breakdown manifests as negative time steps when advancing to a higher atmospheric mass. This unphysical result has no deep significance, as the neglected luminosity is already large enough to give inaccurate results. Sometimes this breakdown occurs even before the crossover mass is reached, although still significantly after growth has started to accelerate. In our models the breakdown occurs at lower atmosphere mass as the semimajor axis increases, since accelerated and eventually runaway growth occurs sooner at larger distances, as seen in Fig. 4. The main practical effect of this behavior is that we halt the evolution where the model breaks down whenever we cannot reach the crossover mass. Fortunately, the elapsed time to either the crossover mass or the breakdown is well-behaved and, most importantly, dominated by lower atmospheric masses where the model is accurate.

5. CRITICAL CORE MASS

5.1. *Disk Temperature and Pressure*

6. NEGLECTED EFFECTS

6.1. *Hydrodynamic Effects*

The neglect of hydrodynamical effects in our model is best discussed in terms of the thermal mass, $M_{\rm th}$, and the length scales introduced in §2.2. In the low mass regime, $M_{\rm p} < M_{\rm th}/\sqrt{3}$, where $R_{\rm B} < R_{\rm H}$, we assume that hydrostatic balance holds out to the outer boundary at $R_{\rm H}$. In this low mass regime, Ormel (2013) calculated the flow patterns driven by stellar tides and disk head-

winds. On scales $\gtrsim R_{\rm B}$ the flows no longer circulate the planet: they belong to the disk. Nevertheless, the density structure outside $R_{\rm B}$ remains spherically symmetric and hydrostatic. Even if these flows do not destroy hydrostatic balance, they could affect the planet's cooling. We expect such effects to be weak, as heat losses at greater depths dominate planetary cooling, but more study is needed.

At higher masses, non-hydrostatic effects become more severe. At $M_{\rm p} \gtrsim M_{\rm th}$ planets can open significant gaps (Zhu et al. 2013). At yet higher masses accretion instabilities could occur (Ayliffe & Bate 2012). However, in this high mass regime we already know that the spherically symmetric approximation breaks down (see §2.2).

Thus by restricting our attention to low masses, neglected hydrodynamic effects should be minor. Moreover since $M_{\rm th} \propto a^{6/7}$ increases with disk radius, spherical hydrostratic models like ours have a greater range of applicability in the outer regions of disks.

6.2. *Realistic Opacities*

Real dust opacities exhibit a more complicated behavior that depends on grain composition. Opacities drop by order unity when ice grains sublimate for $T \gtrsim 150$ K and they drop by orders of magnitude when silicate grains evaporate above $T \gtrsim 1500$ K (Semenov et al. 2003; Ferguson et al. 2005). Our model assumes that radiative regions only exist in the outer part of the atmosphere. As such, even though protoplanetary atmospheres get significantly hotter than 1500 K, our model depends on opacity only in the upper radiative zones, which are cool enough to remain dusty. For our opacity approximations to be valid, we must restrict our model to the lower temperatures of the outer disk.

A second radiative zone inside the convection zone, a "radiative window," is possible, due to the opacity drops caused by the evaporation of ice and metal grains. Our two-layer model ignores such complications. Grain growth also impacts the opacity in the outer regions as well as the existence or depth of radiative windows. We explore more realistic opacity laws in In Piso et al. (2013, in prep.).

6.3. *Equation of State*

In our model we assume an ideal gas law and a polytropic EOS, given by equations (13a) and (13b), respectively. However, non-ideal effects such as partial dissociation and ionization have to be taken into account. One solution is using tabulated equation of state tables for hydrogen and helium mixtures. In Piso et al. (2013, in prep) we use the Saumon et al. (1995) EOS tables and extend them to lower pressures and temperatures as required by our disk assumptions.

7. SUMMARY

In this paper we build evolutionary models of giant planets forming in a protoplanetary disk. We consider atmosphere growth around a core of fixed mass, and determine the minimum core mass for which unstable atmosphere collapse occurs before the dissipation of the protoplanetary disk, at various locations in the disk. For a standard ISM power-law opacity and a polytropic EOS for the nebular gas, the minimum core mass is $\sim 8 M_\oplus$ at 5 AU and decreases to $\sim 3.5 M_\oplus$ at 100 AU. A larger mean molecular weight of the nebular gas increases the critical core mass, while a factor of ten reduction in opacity results in a critical core mass twice as low. Our results are applicable in the outer regions of the disk ($\gtrsim 5$ AU), where planets can undergo runaway gas accretion before opening a gap in the disk. If follows that core accretion at wide separations may result in massive gas giants, which could explain the formation of some of the directly imaged giant planets (Marois et al. 2008; Kalas et al. 2008; Lagrange et al. 2010).

Our results are lower than the typically quoted critical core mass of 10 $M_\oplus$ in static studies. A giant planet can thus form faster if the core grows first, then accretion of solids slows down and a massive atmosphere accumulates, rather than if the core and envelope grow simultaneously in a high planetesimal accretion rate regime. We note that our model is a limiting case of core accretion, in which planetesimal accretion is negligible and the evolution of the gaseous envelope is dominated by KH contraction. We are thus able to place robust absolute lower limits on the core mass needed to form a giant planet, since additional core growth and heating limit the ability of the atmosphere to radiate energy and cool. Our results are not inconsistent with the existence of ice giants at large distances (such as Uranus and Neptune in our own Solar System), as ongoing accretion of solids can stall atmospheric growth and prevent the accumulation of a massive envelope before disk dissipation.

REFERENCES

Alibert, Y., Mordasini, C., Benz, W., & Winisdoerffer, C. 2005, A&A, 434, 343
Arras, P., & Bildsten, L. 2006, ApJ, 650, 394
Ayliffe, B. A., & Bate, M. R. 2012, MNRAS, 427, 2597
Bell, K. R., & Lin, D. N. C. 1994, ApJ, 427, 987
Bodenheimer, P., & Pollack, J. B. 1986, Icarus, 67, 391
Boss, A. P. 1997, Science, 276, 1836
Chiang, E., & Youdin, A. N. 2010, Annual Review of Earth and Planetary Sciences, 38, 493
D'Angelo, G., Durisen, R. H., & Lissauer, J. J. 2011, Giant Planet Formation, ed. S. Piper, 319–346
Dones, L., & Tremaine, S. 1993, Icarus, 103, 67
Ferguson, J. W., Alexander, D. R., Allard, F., Barman, T., Bodnarik, J. G., Hauschildt, P. H., Heffner-Wong, A., & Tamanai, A. 2005, ApJ, 623, 585
Fortney, J. J., Marley, M. S., & Barnes, J. W. 2007, ApJ, 659, 1661
Harris, A. W. 1978, in Lunar and Planetary Institute Science Conference Abstracts, Vol. 9, Lunar and Planetary Institute Science Conference Abstracts, 459–461
Hubickyj, O., Bodenheimer, P., & Lissauer, J. J. 2005, Icarus, 179, 415
Ikoma, M., Nakazawa, K., & Emori, H. 2000, ApJ, 537, 1013
Kalas, P., et al. 2008, Science, 322, 1345
Kenyon, S. J., & Bromley, B. C. 2009, ApJ, 690, L140
Kippenhahn, R., & Weigert, A. 1990, Stellar Structure and Evolution
Kratter, K. M., Murray-Clay, R. A., & Youdin, A. N. 2010, ApJ, 710, 1375
Lagrange, A.-M., et al. 2010, Science, 329, 57
Lambrechts, M., & Johansen, A. 2012, A&A, 544, A32
Marleau, G.-D., & Cumming, A. 2013, arXiv:1302.1517
Marois, C., Macintosh, B., Barman, T., Zuckerman, B., Song, I., Patience, J., Lafrenière, D., & Doyon, R. 2008, Science, 322, 1348
Menou, K., & Goodman, J. 2004, ApJ, 606, 520
Mizuno, H., Nakazawa, K., & Hayashi, C. 1978, Progress of Theoretical Physics, 60, 699
Ormel, C. W. 2013, MNRAS, 428, 3526
Papaloizou, J. C. B., & Nelson, R. P. 2005, A&A, 433, 247

Pollack, J. B., Hubickyj, O., Bodenheimer, P., Lissauer, J. J., Podolak, M., & Greenzweig, Y. 1996, Icarus, 124, 62
Rafikov, R. R. 2005, ApJ, 621, L69
—. 2006, ApJ, 648, 666
Saumon, D., Chabrier, G., & van Horn, H. M. 1995, ApJS, 99, 713
Semenov, D., Henning, T., Helling, C., Ilgner, M., & Sedlmayr, E. 2003, A&A, 410, 611
Stevenson, D. J. 1982, Planet. Space Sci., 30, 755
Youdin, A. N., & Kenyon, S. J. 2013, From Disks to Planets, ed. T. D. Oswalt, L. M. French, & P. Kalas, 1
Youdin, A. N., & Mitchell, J. L. 2010, ApJ, 721, 1113
Zhu, Z., Stone, J. M., & Rafikov, R. R. 2013, ApJ, 768, 143

APPENDIX

A. DERIVATION OF THE GLOBAL ENERGY EQUATION

To derive the global energy equation (17) for an embedded protoplanet, we generalize the analogous calculations in stellar structure theory, e.g. in §4.3 of Kippenhahn & Weigert (1990). For our problem, we add the effects of finite core radius, surface pressure and mass accretion.We start with the local energy equation (10d) whose more natural form in Lagrangian (mass) coordinates is $\partial L/\partial m = \epsilon - T\partial S/\partial t$. Integrating from the core to a higher shell with enclosed mass M gives:

$$L - L_{\rm c} = \int_{M_{\rm c}}^{M} \frac{\partial L}{\partial m} dm \tag{A1a}$$

$$= \int_{M_{\rm c}}^{M} \left(\epsilon - T\frac{\partial S}{\partial t} \right) dm \tag{A1b}$$

$$= \Gamma - \int_{M_{\rm c}}^{M} \frac{\partial u}{\partial t} dm + \int_{M_{\rm c}}^{M} \frac{P}{\rho^2}\frac{\partial \rho}{\partial t} dm \,, \tag{A1c}$$

with $\Gamma = \int \epsilon dm$ the integral of the direct heating rate and applying the first law of thermodynamics in the final step.

The global energy equation is derived by eliminating the partial time derivatives in Equation (A1c), which are performed at a fixed mass, in favor of total time derivatives, denoted with overdots. For instance, the surface radius R of the shell with enclosed mass M evolves as

$$\dot{R} = \frac{\partial R}{\partial t} + \frac{\dot{M}}{4\pi R^2 \rho_M}, \tag{A2}$$

where $\partial R/\partial t$ gives the Lagrangian contraction of the "original" shell, and mass accretion through the upper boundary at rate $\dot{M}$ also changes the shell location. Similarly, the volume $V = (4\pi/3)R^3$ and pressure at the outer shell evolve as

$$\dot{V}_M = \frac{\partial V_{\rm M}}{\partial t} + \frac{\dot{M}}{\rho_{\rm M}} \tag{A3a}$$

$$\dot{P}_M = \frac{\partial P_{\rm M}}{\partial t} + \frac{\partial P_M}{\partial m}\dot{M} = \frac{\partial P_{\rm M}}{\partial t} - \frac{GM}{4\pi R^4}\dot{M} \,. \tag{A3b}$$

This derivation holds the core mass and radius fixed, $\dot{M}_{\rm c} = \dot{R}_{\rm c} = 0$. Therefore the core pressure satisfies

$$\dot{P}_{\rm c} = \partial P_{\rm c}/\partial t \,. \tag{A4}$$

The internal energy integral follows simply from Leibniz's rule as

$$\int_{M_{\rm c}}^{M(t)} \frac{\partial u}{\partial t} dm = \dot{U} - \dot{M} u_M \,. \tag{A5}$$

To make further progress we use the virial theorem:

$$E_G = -3\int_{M_{\rm c}}^{M} \frac{P}{\rho} dm + 4\pi(R^3 P_M - R_{\rm c}^3 P_{\rm c}), \tag{A6}$$

which follows from Equations (10a), (10b) and (15) by integrating hydrostatic balance in Lagrangian coordinates. As an aside, the integral in equation (A6) can be evaluated for a polytropic EOS to give simple expressions for the total energy:

$$E = (1-\zeta)U + 4\pi(R^3 P_M - R_{\rm c}^3 P_{\rm c}) \tag{A7a}$$

$$= \frac{\zeta - 1}{\zeta} E_G + \frac{4\pi}{\zeta}(R^3 P_M - R_{\rm c}^3 P_{\rm c}) \tag{A7b}$$

where $\zeta \equiv 3(\gamma - 1)$. We will not make this assumption and will keep the EOS general.

To express the work integral, the final term in Equation (A1c), in terms of changes to gravitational energy we first take the time derivative of Equation (A6):

$$\dot{E}_G = 3\int_{M_c}^{M} \frac{P}{\rho^2}\frac{\partial \rho}{\partial t} dm - 3\int_{M_c}^{M} \frac{\partial P}{\partial t}\frac{dm}{\rho} - 3\frac{P_M}{\rho_M}\dot{M} + 3\dot{P}_M V_M - 3\dot{P}_c V_c + 3P_M \dot{V}_M \,. \tag{A8}$$

The first integral in Equation (A8) is the one we want, but the next one must be eliminated. The time derivative of Equation (15) (times four) gives

$$\begin{aligned} 4\dot{E}_G &= -4\frac{GM\dot{M}}{R} + 4\int_{M_c}^{M} \frac{Gm}{r^2}\frac{\partial r}{\partial t} dm & \text{(A9a)} \\ &= -4\frac{GM\dot{M}}{R} + 4\pi\int_{M_c}^{M} r^3 \frac{\partial}{\partial m}\frac{\partial P}{\partial t} dm & \text{(A9b)} \\ &= -4\frac{GM\dot{M}}{R} - 3\int_{M_c}^{M} \frac{\partial P}{\partial t}\frac{dm}{\rho} + 3V_M\frac{\partial P_M}{\partial t} - 3V_c\frac{\partial P_c}{\partial t} & \text{(A9c)} \end{aligned}$$

where Equations (A9b) and (A9c) use hydrostatic balance and integration by parts.

Subtracting Equations (A5) and (A9c) and rearranging terms with the help of Equations (A2), (A3) and (A4) gives

$$\int_{M_c}^{M} \frac{P}{\rho^2}\frac{\partial \rho}{\partial t} dm = -\dot{E}_G - \frac{GM\dot{M}}{R} - P_M\frac{\partial V_M}{\partial t} \,. \tag{A10}$$

Combining Equations (A1c), (A5) and (A10), we reproduce Equation (17) with the accreted specific energy $e_M \equiv u_M - GM/R$.

B. ANALYTIC COOLING MODEL DETAILS

B.1. *Isothermal Atmosphere*

We consider the structure of a non self-gravitating isothermal atmosphere that extends outward from the radiative-convective boundary RCB and matches onto the disk density, ρ_d, at a distance $r_{fit} = n_{fit} R_B$, where R_B is the Bondi radius defined in equation (7). From equation (10b) the resulting density profile is

$$\rho = \rho_d \exp\left(\frac{R_B}{r} - \frac{1}{n_{fit}}\right) \approx \rho_d \exp\left(\frac{R_B}{r}\right), \tag{B1}$$

where the approximate inequality is valid deep inside the atmosphere ($r \ll R_B$) for any $n_{fit} \gtrsim 1$. However, the choice of boundary condition does have an order unity effect on the density near the Bondi radius.

The mass of the atmosphere is determined by integrating equation (10a) from the RCB to the Bondi radius using the density profile (B1) and can be approximated as

$$M_{iso} \approx 4\pi\rho_d \frac{R_{RCB}^4}{R_B} e^{R_B/R_{RCB}} = 4\pi\rho_{RCB}\frac{R_{RCB}^4}{R_B} \tag{B2}$$

with ρ_{RCB} the density at the RCB. This result is the leading order term in a series expansion. By comparing the expression above and Equation (27) under the assumption that $R_{RCB} \ll R_B$, we see that the mass of the outer radiative region (which is nearly isothermal) is negligible when compared with the atmosphere mass in the convective layer, as stated in section §3.

B.2. *Temperature and Pressure Corrections at the Radiative-Convective Boundary*

In this section we estimate the temperature and pressure corrections at the RCB due to the fact that the radiative region is not purely isothermal. From equation (11), we express the radiative lapse rate

$$\nabla_{rad} = \frac{3\kappa P}{64\pi GM\sigma T^4} L = \nabla_d \frac{P/P_d}{(T/T_d)^{4-\beta}}, \tag{B3}$$

where the second equality follows from the opacity law (5) and ∇_d is the radiative temperature gradient at the disk:

$$\nabla_d \equiv \frac{3\kappa(T_d)P_d}{64\pi GM\sigma T_d^4} L. \tag{B4}$$

Here M is the total planet mass. Since our analytic model neglects self-gravity, $M = M_c$ and therefore ∇_d is constant. From equation (B3) and $\nabla_{rad} = d\ln T/d\ln P$, the temperature profile in the radiative region integrates to

$$\left(\frac{T}{T_d}\right)^{4-\beta} - 1 = \frac{\nabla_d}{\nabla_\infty}\left(\frac{P}{P_d} - 1\right), \tag{B5}$$

where $\nabla_\infty = 1/(4-\beta)$ is the radiative temperature gradient for $T, P \to \infty$. Applying Equations (B3) and (B5) at the RCB (where $\nabla_{\rm rad} = \nabla_{\rm ad}$) under the assumption that $P_{\rm RCB} \gg P_{\rm d}$ results in $T_{\rm RCB} = \chi T_{\rm d}$ as in Equation (20a), with χ defined in Equation (21).

The pressure at the RCB follows from Equations (B5) and (20a) as

$$\frac{P_{\rm RCB}}{P_{\rm d}} \simeq \frac{\nabla_{\rm ad}/\nabla_{\rm d}}{1 - \nabla_{\rm ad}/\nabla_\infty}. \tag{B6}$$

We can eliminate $\nabla_{\rm d}$ from equation (B6) to obtain a relation between temperature and pressure in the radiative zone as a function of the RCB pressure $P_{\rm RCB}$. From Equation (B5), it follows that

$$\frac{T}{T_{\rm d}} = \left[1 + \frac{1}{\frac{\nabla_\infty}{\nabla_{\rm ad}} - 1}\left(\frac{P}{P_{\rm RCB}} - \frac{P_{\rm d}}{P_{\rm RCB}}\right)\right]^{\frac{1}{4-\beta}}. \tag{B7}$$

We can then determine the radius of the convective boundary $R_{\rm RCB}$ from the Equation (10b) as

$$\frac{R_B}{R_{\rm RCB}} = \int_{P_{\rm d}}^{P_{\rm RCB}} \frac{T}{T_{\rm d}} \frac{dP}{P}. \tag{B8}$$

Evaluating the integral leads to

$$\frac{R_B}{r_{\rm RCB}} = \ln\left(\frac{P_{\rm RCB}}{P_{\rm d}}\right) - \ln\theta, \tag{B9}$$

with an extra correction term $\theta < 1$, when compared to an isothermal atmosphere (see Equation B1). From this we arrive at the relation between $P_{\rm RCB}$ and $P_{\rm d}$ given by Equation (20b). As opposed from the temperature correction factor χ, an analytic expression for θ cannot be obtained. Estimates for χ and θ for different values of the exponent β in the opacity law (5) are presented in Table 1.

B.3. *The Opacity Effect*

A lower opacity decreases the critical core mass. Reducing the opacity by a factor of one hundred results in a critical core mass one order of magnitude lower than in the standard ISM case, specifically $M_{\rm crit} \approx 9 M_\oplus$ for the parameters in Equation (37). The reduction is not as strong as the nominal scaling would imply, $0.01^{3/5} \approx 0.06$, because ξ increases.

Even with significantly lower opacities, radiative diffusion remains a good approximation at the RCB. For $\beta = 2$, we estimate the optical depth as

$$\tau_{\rm RCB} \sim \frac{\kappa_{\rm RCB} P_{\rm RCB}}{g} \sim 7 \times 10^4 \frac{F_T^4 F_\kappa}{\left(\frac{m_{\rm c\oplus}}{10}\right)\left(\frac{a_\oplus}{10}\right)^{\frac{12}{7}}}, \tag{B10}$$

where $P_{\rm RCB} \sim P_M$ for a self-gravitating atmosphere and $g \sim G M_{\rm c}/R_B^2$, with both approximations good to within the order unity factor ξ. We see that $\tau_{\rm RCB} \gg 1$ even for $F_\kappa \lesssim 0.01$ out to very wide separations, hence the atmosphere remains optically thick at the RCB.

B.4. *Surface Terms*

In this section we check the relevance of the neglected surface terms in Equation (17). We first show that accretion energy is only a small correction at the RCB, which is where we apply our cooling model. A rough comparison (ignoring terms of order ξ) of accretion luminosity vs. $\dot{E}$ gives

$$\frac{GM\dot{M}}{R\dot{E}} = \frac{GM}{R}\frac{dM}{dE} \sim \frac{GM_{\rm c}^2}{R_B E}\frac{P_{\rm RCB}}{P_M} \sim \sqrt{\frac{R_{\rm c}}{R_B}} \ll 1, \tag{B11}$$

where we assume $P_{\rm RCB} \sim P_M$ for a massive atmosphere. Accretion energy at the protoplanetary surface is thus very weak for marginally self-gravitating atmospheres, and even weaker for lower mass atmospheres. A similar scaling analysis shows that the work term $P_M \partial V_M/\partial t$ is similarly weak. Nevertheless, our numerical calculations include these surface terms in a more realistic and complete model of self-gravitating atmospheres.

TABLE 1
Parameters Describing Structure of Radiative Zone.

$\gamma = 7/5$ ($\nabla_{\rm ad} = 2/7$)					
β	1/2	3/4	1	3/2	2
∇_∞	2/7 [a]	4/13	1/3	2/5	1/2
χ	···	2.25245	1.91293	1.65054	1.52753
θ	···	0.145032	0.285824	0.456333	0.556069

[a] Since $\nabla_{\rm ad} = \nabla_\infty$ there is no convective transition at depth for this case.